Medwell, Paul Ross; Chan, Qing Nian; Kalt, Peter Anthony Markus; Alwahabi, Zeyad; Dally, Bassam; Nathan, Graham Jerrold.
Development of temperature imaging using two-line atomic fluorescence, *Applied Optics*, 2009; 48(6):1237-1248.

Development of temperature imaging using two-line atomic fluorescence

Paul R. Medwell,[1,*] Qing N. Chan,[1,2] Peter A. M. Kalt,[1] Zeyad T. Alwahabi,[2] Bassam B. Dally,[1] and Graham J. Nathan[1]

[1]School of Mechanical Engineering, The University of Adelaide, S.A. 5005 Australia

[2]School of Chemical Engineering, The University of Adelaide, S.A. 5005 Australia

*Corresponding author: paul.medwell@adelaide.edu.au

Received 5 November 2008; revised 18 January 2009; accepted 21 January 2009; posted 21 January 2009 (Doc. ID 103719); published 20 February 2009

This work aims to advance understanding of the coupling between temperature and soot. The ability to image temperature using the two-line atomic fluorescence (TLAF) technique is demonstrated. Previous TLAF theory is extended from linear excitation into the nonlinear fluence regime. Nonlinear regime two-line atomic fluorescence (NTLAF) provides superior signal and reduces single-shot uncertainty from 250 K for conventional TLAF down to 100 K. NTLAF is shown to resolve the temperature profile across the stoichiometric envelope for hydrogen, ethylene, and natural gas flames, with deviation from thermocouple measurements not exceeding 100 K, and typically $\lesssim$30 K. Measurements in flames containing soot demonstrate good capacity of NTLAF to exclude interferences that hamper most two-dimensional thermometry techniques.

OCIS codes: 120.1740, 120.6780, 300.2530.

1. Introduction

Soot is one of the key elements of many combustion systems. Soot plays an important, and highly effective, role in radiative heat transfer. Radiation from soot is typically the dominant heat transfer mode in boilers and furnaces [1,2]. Soot is also a commercial product ($>10^7$ tons per annum) used for several applications, including elastomers, tires, and ink [3]. On the other hand, soot is an unsightly emission from combustion processes and presents a major environmental pollutant and health risk [4,5]. A comprehensive understanding of the chemical and physical processes involved in soot formation and oxidation is therefore essential, not only from a fundamental scientific standpoint, but also the application in practical combustion systems. To further understand the complex soot formation and oxidation process in a turbulent environment, there is a need for the parallel application of accurate measurements and the development of models that are rigorously tested against reliable data sets. A multitude of interdependent parameters are of fundamental importance to soot; however, temperature remains one of the most significant in controlling the chemical reactions and physical processes in combustion systems [6]. The present paper addresses the need for accurate temperature measurements in the difficult conditions associated with soot.

Laser-based techniques have supplied the combustion research community with *in situ* instantaneous, nonintrusive, temporally and spatially precise measurement of many important parameters of interest [7]. Producing experimental data sets in flames containing soot using laser-based techniques has been problematic, however [8]. Absorption, scatter, and other interferences due to the presence of soot and its precursors in such flames prevent many laser diagnostic techniques, such as Rayleigh scattering, from being applied reliably to such flames. These issues lead to the application of laser diagnostics often being limited to idealized clean flames, thus excluding many flames of practical significance. It is

0003-6935/09/061237-12$15.00/0

therefore apparent that there is a need for alternative temperature measurement techniques to complement and extend those already in common use.

One of the most experimentally simple, yet useful, laser-based temperature techniques is Rayleigh scattering. The elastic scatter of light from molecules gives a measure of the total number density, which, when coupled with the ideal gas law, allows the temperature to be deduced. Rayleigh scattering measurements can only be employed under very clean, particle-free situations, because the elastic nature of the process is highly susceptible to interference from spurious Mie scatter [9]. Filtered Rayleigh scatter is less susceptible to interference [10–12] but remains impractical for highly particle-laden flows.

To circumvent problems associated with elastic scatter, Raman-based thermometry is possible using various approaches [9]. The inherently low signal associated with Raman does restrict the application of spontaneous Raman approaches to thermometry due to issues with signal quality and is typically limited to line measurements. Offering stronger signal, and more applicable to luminous and particle-laden flows, coherent anti-Stokes Raman spectroscopy (CARS)-based thermometry is highly advantageous [13]. Nonetheless, the necessity for line-of-sight optical access, the experimental complexity (including effects of laser mode), and the lack of spatial fidelity in comparison to planar techniques does restrict the generic application of CARS [7].

Various laser-induced fluorescence (LIF) strategies exist for thermometry, all of which are based on the species' population according to the Boltzmann distribution. LIF-based techniques can use either naturally occurring species or a seeded species. The fluorescence signal is typically quite strong, making LIF better suited to two-dimensional imaging than other techniques (e.g., spontaneous Raman). The frequency shift associated with the fluorescence process is advantageous for reducing interference, especially in comparison to Rayleigh scattering.

The use of *in situ* species for LIF thermometry is limited because of low concentrations of many potential species (e.g., OH, CN, and CH) and the narrow regions within the flame in which many species exist. Of the naturally occurring species within a flame, the OH radical is one of the most commonly used [8,14–16]. In nonpremixed flames, OH only exists over a small range of temperature and mixture fraction, and so is not well suited for general measurements [17]. Furthermore, in fuel-rich flames, the OH concentration is low so that it is poorly suited to simultaneous measurements with soot, which is typically found in the fuel-rich side of the reaction zone [18]. Nitric oxide (NO), which is formed natively during the combustion process, could potentially be used for thermometry, though additional NO is typically added to the inlet streams to give a much improved signal quality [8,19]. However, in the presence of soot, background interferences can lead to a significant error in two-line NO-LIF thermometry [20]. Multiline approaches for NO thermometry alleviate issues with background [21] but at the cost of being restricted to averaged results. The excitation wavelengths required for NO (around 226 nm) can also cause problems with interference and attenuation, and pressure broadening of the excitation lines leads to spectral overlap [22]. Furthermore, in fuel-rich flames, NO is consumed due to reburn reactions, leading to a loss of signal [19,23].

Of the laser-based thermometry techniques, two-line atomic fluorescence (TLAF) is potentially one of the most suitable for sooting environments, especially for two-dimensional imaging [7]. TLAF follows the same principle as other LIF-based thermometry techniques but uses a seeded atomic species. Some advantages of the TLAF technique include [24–27] good sensitivity over a temperature range relevant to combustion, insensitivity to collisional quenching effects, and the inelastic nature enables filtering to minimize interferences from spurious scattering. Of the atomic species available, indium seeded into the flame has been identified as a suitable thermometry species for TLAF (e.g., [28]). Indium has good sensitivity over the temperature range ~800–2800 K [29] and both wavelengths are in the visible (namely, 410 and 450 nm), where interferences are less pronounced than in the UV range, where many spectral species need to be excited. Recent feasibility studies [17,27] have shown that TLAF with indium holds promise for temperature measurement in a highly sooting environment. The indium is introduced to the system as indium chloride, which is dissolved in water. Within the flame front, neutral indium atoms are generated, which are spectroscopically probed using the TLAF technique.

The theory was first evaluated by Alkemade [30] and has subsequently been the interest of other studies [17,24,27,29,31,32]. The TLAF technique is based on the optical excitation of two electronic transitional energy states and the sequential detection of the spectrally shifted emission. The ratio of the two fluorescence signals is subsequently used to ascertain the relative population in each of the two energy levels based on the Boltzmann distribution function.

Conventional TLAF is based on the excitation and subsequent detection of two wavelengths. These can be synchronized in sufficiently close succession (a few hundred nanoseconds) to provide effectively instantaneous temperature imaging in turbulent flows, whose motions are typically at the millisecond timescale. As a slight variation on the technique, instead of using only two wavelengths, scanning is possible. In such a situation, a narrowband tunable laser is used to scan over the absorption lines, and the detected spectra can be used to determine the temperature based on a fit of the resultant curve [32–34]. The scanning approach has the advantage of being self-calibrating, but the scanning is not instantaneous and so yields only averaged temperature measurements.

Previous TLAF theory has been limited to low laser fluence [27], whereby the relationship between the excitation fluence and the resulting fluorescence signal is linear. Under such conditions, the signal is plagued by low signal-to-noise, thus preventing useful single-shot imaging. Of the few studies that have applied TLAF, time-averaged results have typically been reported. With some notable exceptions (e.g., [29]), virtually all past work on TLAF has been performed in laminar premixed flames, and thus the limitation of measuring mean temperature has been acceptable. In the context of turbulent flames, however, such averaged data are insufficient.

The present study aims to develop the TLAF technique to improve a sufficient signal-to-noise ratio (SNR) to allow instantaneous temperature imaging in turbulent environments. The SNR of TLAF in the linear fluence excitation regime is assessed. One approach to achieve the SNR is to extend the fluence into the nonlinear regime. For work in the nonlinear regime, simplifications made in previously developed linear TLAF theory no longer hold. Derivations are made to facilitate the application of nonlinear regime two-line atomic fluorescence (NTLAF). The developed NTLAF technique is used to measure the flame temperature of three different fuel types across a range of operating conditions. For assessment of the NTLAF method, a laminar premixed burner is used. This avoids the complexities associated with turbulent and/or nonpremixed flames. Future studies will seek to extend this method to turbulent flames with simultaneous measurement of soot.

2. Methodology

The TLAF technique is based on the optical excitation of two electronic transitional states and the sequential detection of the spectrally shifted emission. Figure 1 diagrammatically shows the three energy levels of neutral indium atoms (In) that are relevant to TLAF. Two transitions to the excited $6^2S_{1/2}$ level are possible, one each from $5^2P_{1/2}$ and $5^2P_{3/2}$, corresponding to 410.18 and 451.13 nm, respectively [35].

The TLAF excitation/detection process consists of two distinct operations. The Stokes transition requires 410 nm laser excitation, and the subsequent fluorescence is detected at 450 nm. The anti-Stokes process is excited at 450 nm and emits at 410 nm. By introducing a small time delay (of the order of 100 ns) between the two excitation pulses, in conjunction with optical filtering, the Stokes fluorescence detected at 450 nm may be essentially immune from spurious scatter from the anti-Stokes excitation at that same wavelength. The same applies for the 410 nm Stokes excitation and anti-Stokes emission. By both temporally and spectrally shifting the Stokes and anti-Stokes processes, measurements in sooting conditions are potentially feasible.

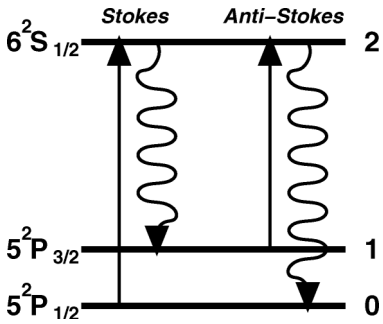

Fig. 1. (Color online) TLAF energy transitions.

By applying the rate equation for pumping to level 2 via optical absorption from the lower states, in conjunction with the fluorescence from level 2 to the lower states, and incorporating the Boltzmann distribution, it is shown that, in the linear excitation regime, the temperature is given by [31]

$$T = \frac{\Delta E_{10}/k}{\ln\left(\frac{F_{21}}{I_{02}}\right) - \ln\left(\frac{F_{20}}{I_{12}}\right) + 4\ln\left(\frac{\lambda_{21}}{\lambda_{20}}\right) + C_t}. \quad (1)$$

Here ΔE is the energy difference between levels, F is the fluorescence, I is the laser spectral irradiance, λ is the wavelength, and C_t is a constant dependent on a number of experimental factors (such as collection efficiency) and is best determined from experimental calibration. The subscripts refer to the transition between the energy levels (Fig. 1).

Equation (1) and previous TLAF studies rely on the assumption of excitation in the linear LIF regime. To improve the fluorescence signal, there are potential advantages in extending the fluence beyond the linear limit. In this case, the previously defined theory and derivations will no longer apply. Without any simplifications resulting from linearity assumptions, the derivation of the temperature follows a similar procedure but includes two additional parameters that result in the equation being independent of the fluence regime. Following the derivation given in Appendix A, the equation for NTLAF takes the form

$$T = \frac{\Delta E_{10}/k}{\ln\left(F_{21}\times\left(1+\frac{C_S}{I_{20}}\right)\right) - \ln\left(F_{20}\times\left(1+\frac{C_A}{I_{21}}\right)\right) + C_T}, \quad (2)$$

where the parameters C_S, C_A, and C_T are defined as

$$C_S = \frac{Q+A}{B_{20}}, \quad (3)$$

$$C_A = \frac{Q+A}{B_{21}}, \quad (4)$$

$$C_T = \ln\left(\frac{\nu_{20}}{\nu_{21}}\right) + \ln\left(\frac{\Omega_{20}}{\Omega_{21}}\right) + \ln\left(\frac{\varepsilon_{20}}{\varepsilon_{21}}\right) + \ln\left(\frac{A_{20}}{A_{21}}\right). \quad (5)$$

C_A and C_S can be derived experimentally from a fluorescence versus irradiance plot for the two

(Stokes and anti-Stokes) excitation schemes, while C_T is determined via calibration.

3. Experimental Setup

A. Experimental Overview

The experimental arrangement is shown in Fig. 2. Two Nd:YAG-pumped dye lasers are fired nearly simultaneously (~100 ns separation) to produce the 410.18 and 451.13 nm excitation beams, with linewidths of 0.4 and 0.3 cm^{-1}, respectively. The 410 nm wavelength is achieved by pumping a mixture of Pyridine 1 and DCM dye at 532 nm (generating ~667 nm) and mixing with the residual 1064 nm, while the 451 nm is the output of a 355 nm pumped mixture of Coumarin 450 and Coumarin 460 dyes. Using the difference in polarization, the 410 and 450 nm beams are combined, converted to circular polarization, and shaped into a coplanar sheet of 45 mm height and ~4.5 mm thickness. Circular polarization is favored to prevent bias in the detected signal due to the difference in linear polarization orientation of the beams. A thick light sheet gives an improved SNR and is sufficient for the current laminar flat-flame burner. However, future experiments with turbulent flames will require a thinner light sheet ($\lesssim$0.5 mm).

The laser beams are directed through a glass tank in the same field of view as the premixed flat-flame burner (Subsection 3.B). The tank is filled with fluorescing dye and facilitates correction of laser energy variation across the sheet height and between laser pulses. From both the tank and the flame, the frequency-shifted fluorescence is detected through 10 nm bandwidth interference filters (centered at 410 and 450 nm) using two intensified CCD cameras with $f_{\#}$1.4 lenses. The camera gate width of 50 ns is synchronized to the opposite wavelength excitation laser pulse to avoid interference from elastic scatter. The resultant images from each of the cameras are spatially matched with software using a three-point matching algorithm during image processing to ensure a sufficient overlap of the corresponding images. Measurements were conducted 20 mm above the burner face to provide a uniform thermal field away from any interference from the burner.

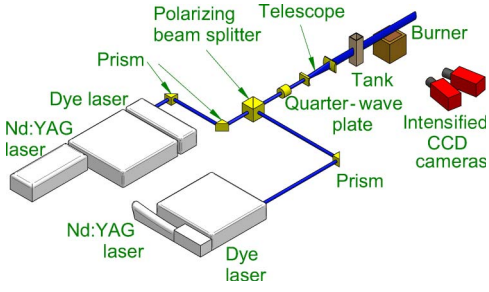

Fig. 2. (Color online) Schematic of experimental layout.

B. Burner and Seeding Arrangements

In this study, a laminar premixed flat-flame burner is used as shown in Fig. 3. The burner face measures 50 mm × 50 mm and consists of a series of tubes (ø1.6 mm) fueled with a premixture of fuel, air, and nitrogen. The nitrogen acts as a carrier gas to facilitate the seeding of indium. The seeder consists of an ultrasonic nebulizer, which generates a mist of 5 μm diameter droplets of indium chloride dissolved in distilled water. To damp variations in the aerosol generation, a ballast volume is included between the seeder and the burner [36].

Various fuel types are considered in this paper, namely, natural gas ($\gtrsim$92% CH_4), hydrogen, and ethylene. The conditions for two selected natural gas/air flames are shown in Table 1 along with the range of conditions for the other flames. Much of the data presented in this paper are shown for a range of stoichiometries (Φ). In such cases, Φ was adjusted by varying the fuel flow rate at a constant oxidant flow rate to maintain a similar volumetric flow rate (and thus similar seeded indium concentration).

4. Results and Discussion

A. Linear Fluence

The SNR of the indium fluorescence images is dependent on the laser energy used. To optimize the SNR in this regime, it is necessary to identify the transition from a linear to a nonlinear response.

To determine the maximum fluence before deviation from the linear regime, the indium fluorescence is plotted against the excitation energy for both excitation schemes. To generate such a plot, the laser energy was varied by the addition of neutral density filters of differing optical density. This approach maintains consistent optical properties of the laser while changing the fluence. The flame conditions and indium seeding concentration are held constant.

Figure 4 presents the (200 shot) average of both Stokes and anti-Stokes indium fluorescence obtained for Flame 1 (Table 1) for various laser energies and thus spectral irradiances. Also included on this plot is the standard deviation for each point. It is apparent that the fluorescence is linear for a laser energy of up to 2500 $W/cm^2/cm^{-1}$, beyond which nonlinear behavior is detected. An irradiance of ~3000 $W/cm^2/cm^{-1}$ has previously been indicated to be in the linear

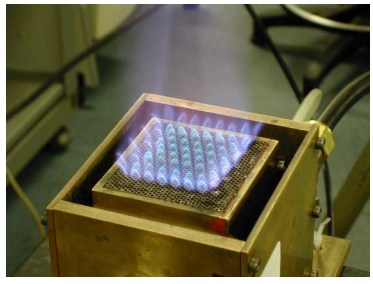

Fig. 3. (Color online) Photograph of Flame 1 (Table 1) and burner. Burner face measures 50 mm × 50 mm.

Table 1. Premixed Flat-Flame Conditions

Flame Mode	Fuel Type	Stoichiometry (Φ)	% N_2 (vol/vol)	Bulk Velocity (m/s)	Temperature (K)
1	Natural gas	1.5	18	0.17	1803
2	Natural gas	1.2	14	0.23	2004
3	Natural gas	0.93–1.46	10.0–10.5	0.30–0.32	1810–2033
4	Hydrogen	0.94–3.78	16–28	0.11–0.20	1082–1578
5	Ethylene	0.80–2.25	9.9–17	0.19–0.32	1589–2246

excitation regime [17,27], consistent with our current validation.

B. Seeding Concentration

The fluorescence signal is dependent on the number of neutral indium atoms present in the probe volume. For the TLAF theory to apply, it is necessary to verify that the fluorescence is linear with the concentration of indium. Figure 5 presents the fluorescence intensity as a function of the concentration of indium chloride in the seeding solution. The indium chloride concentration is assumed to be directly proportional to the number of neutral indium atoms within the flame itself. Shown in Fig. 5 is both the mean and standard deviation of the integrated fluorescence intensity over a 100-shot data set.

Figure 5 demonstrates that, for the current seeding arrangement, the behavior of the fluorescence is linear up to a concentration of 10 mg/mL. Of particular note is that, despite an increase in mean signal with higher concentration, the standard deviation (normalized by the mean) remains approximately constant. This results in there being no net improvement in the SNR with an increase in the concentration of indium. For the remainder of the experimental results presented, a concentration of 1.5 mg/mL is used to ensure linear behavior with concentration while minimizing the effect of indium on the flame properties.

It is advantageous to minimize the seeding concentration, because it has previously been indicated that the presence of metal additives within a flame environment can influence the soot formation process [37]. Although global flame properties remain unaffected, metal ions, when present in sufficient quantity, could inhibit coagulation of soot particles [38], leading to a greater number of small particles and thus to a higher oxidation rate [39]. For low to moderate seeding concentrations, it has been shown using laser-induced incandescence measurements that, within experimental uncertainty, the inclusion of indium does not affect the soot volume fraction [17].

Providing the indium concentration is sufficient to yield good signal, precise determination of the concentration is not overly important since the measurement of temperature using the TLAF theory is independent of the indium concentration. Thermocouple measurements confirm that the inclusion of indium into the flame has a negligible influence on the flame temperature itself, which is below measurable limits.

C. Temperature Calibration

As described in Section 2, to determine temperature from TLAF requires the evaluation of a calibration constant. Thus a reference temperature is required using an independent technique. Here an *R*-type thermocouple (ø0.7 mm) was used as the primary reference. The measured thermocouple temperature was corrected for radiation by applying an energy balance to the junction [6]. To validate the thermocouple measurement, temperature was also measured using Rayleigh scattering and compared with adiabatic equilibrium calculations. The results of the

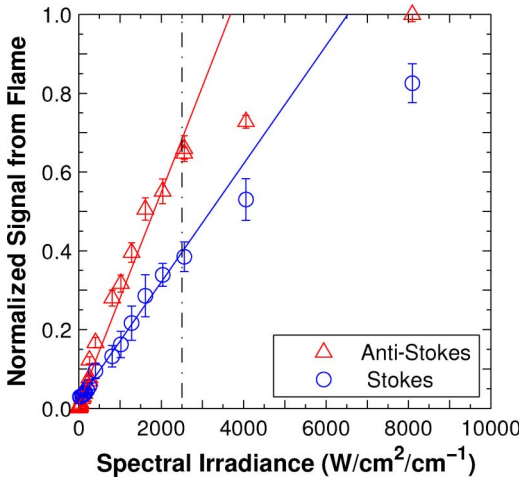

Fig. 4. (Color online) Indium fluorescence as a function of spectral intensity in the linear fluence regime.

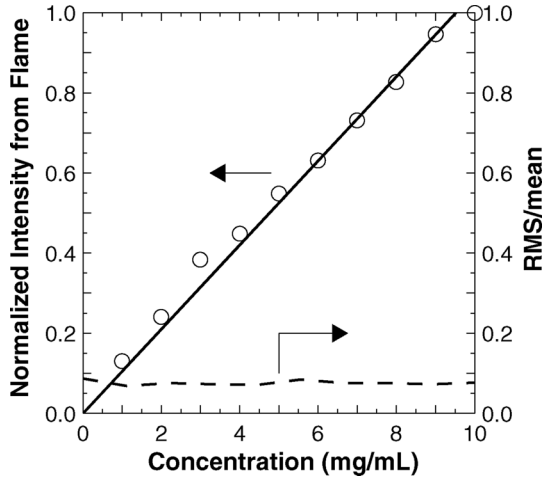

Fig. 5. (Color online) Indium fluorescence as a function of indium chloride concentration.

independently derived maximum temperature obtained for a premixed natural gas/air flame are shown in Table 2. The two measured values agree to within ~10 K. The calculated value agrees with the measured values to ≲30 K. This difference in temperature is expected due to radiative heat loss from the flame, which is not accounted for in the adiabatic equilibrium calculations.

D. Instantaneous Images—Linear Fluence

Figures 6(a) and 6(b) show typical instantaneous images of the Stokes and anti-Stokes indium fluorescence recorded simultaneously under a low spectral irradiance of approximately 2500 $W/cm^2/cm^{-1}$. Each image has been spatially matched and corrected for background and detector attenuation. The images represent an area 20 mm high and 50 mm wide, centered 20 mm above the burner face.

Both the Stokes and anti-Stokes images show a gradient in the indium fluorescence across the width of the flame. An independent measurement of temperature suggests that the thermal field across the measurement volume is essentially constant. The variation in signal is attributed to a variation in the concentration of neutral indium atoms throughout the burner. The nonuniformity of indium atoms is believed to be due to a combination of nonuniform seeding and the process by which the indium atoms are formed from the indium chloride solution. In the context of TLAF, such a difference in concentration only influences the absolute signal and not the deduced temperature. As can be seen in these images, the nonuniformity affects both the Stokes and the anti-Stokes fluorescence, thus the differences cancel out in the temperature expression.

The stoichiometry of the flame presented in Fig. 6 is approximately 1.5, which favors strong indium fluorescence. Previous studies (e.g., [27]) have also shown that fuel-rich conditions provide the optimal environment for maximizing the indium signal. An increase in signal under fuel-rich conditions is attributed to the reducing environment necessary for the conversion of the indium chloride salt to neutral indium atoms [29]. The formation of neutral indium is believed to involve electron–ion recombination and molecular dissociation, though the exact process by which the atoms are produced is complex and unclear [40].

Despite near-optimal flame conditions, the SNR (defined as the ratio of the signal intensity to the interpixel noise) of the instantaneous fluorescence images in Fig. 6 is ~18:1 for Stokes and only ~5:1 for anti-Stokes.

Table 2. Maximum Temperature Measurements and Calculation for a Premixed Natural Gas/Air Flame

Technique	Maximum Temperature (K)
Adiabatic equilibrium calculations	2232
Thermocouple (after radiation correction)	2204
Rayleigh scattering	2211

E. Temperature Measurement—Linear Fluence

From the combination of the instantaneous images presented in Figs. 6(a) and 6(b), the TLAF equation [Eq. (1)], and the calibrated thermocouple temperature, the temperature distribution throughout the image has been calculated in Fig. 6(c). The calibration constant was determined by "forcing" the mean temperature of the averaged images to match the radiation-corrected thermocouple reading at one point of the flow [31]. This calibration method limits the TLAF accuracy to that of a thermocouple (here ±30 K) but does not affect the precision of the technique. Determination of the C_t term in Eq. (1) via calibration is preferred over trying to estimate the necessary terms grouped into the constant. Experimental calibration eliminates the need for accurate quantification of numerous experimental factors, such as laser linewidth, collection efficiency, and seed concentration [31].

Since the calibration constant was chosen based on this particular flame condition, the temperature measurement necessarily agrees with the thermocouple measurement. Nevertheless, the almost uniform temperature distribution appearance, with a slight increase toward the edges of the flame, follows the same trend of that measured using the thermocouple probe. The high apparent temperature and gradient at the edges of the flame is a result of the paucity of indium in the surrounding air. The SNR of the deduced temperature image is approximately 8:1, corresponding to an uncertainty of ~250 K.

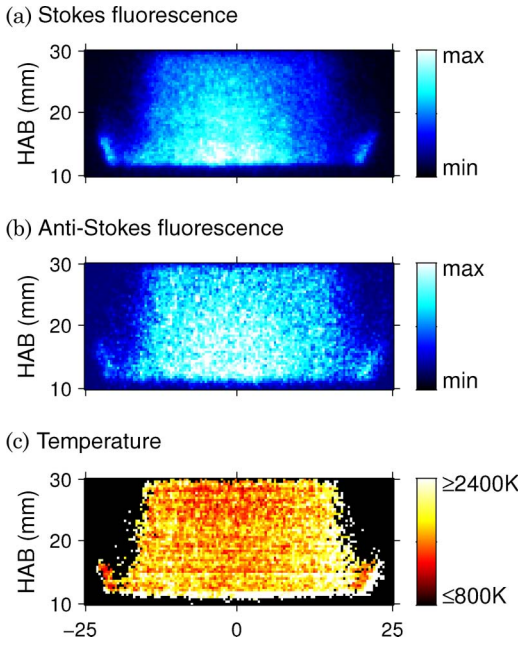

Fig. 6. (Color online) Typical instantaneous images of (a) Stokes and (b) anti-Stokes indium fluorescence and (c) deduced temperature in Flame 1 (Table 1). Linear fluence excitation (2500 $W/cm^2/cm^{-1}$). Image size approximately 20 mm × 50 mm. Laser propagation from left to right. HAB, height above burner.

The SNR of the instantaneous temperature image [Fig. 6(c)] is rather poor. To improve the quality of the image, Fig. 7 presents the deduced temperature for the same conditions but now over a 200-shot average. Being a steady laminar flame, there is no other significant loss of information resulting from the averaging. As a result of the averaging, the SNR is improved to 20:1 (i.e., ~100 K).

To assess the sensitivity of the technique to operating conditions, Fig. 8 shows the averaged temperature image for Flame 2 (Table 1). The calibration constant for Flame 2 is the same as determined for Fig. 7. The TLAF measurement yields a temperature of 2030 K, in good agreement with the thermocouple measurement of 2004 K. Nonetheless, these images remain averaged over 200 shots.

F. Nonlinear Fluence

The linearity-limited spectral irradiance has been shown to be 2.5×10^3 W/cm^2/cm^{-1} (Subsection 4.A). Figure 9 now extends the fluence to 5×10^9 W/cm^2/cm^{-1}, representing the maximum attainable laser power when shaped into a line. Despite an increase in the fluence by 6 orders of magnitude, complete saturation (i.e., to a plateau) does not occur.

It is apparent that there is a potential for a significant improvement in the signal intensity by increasing the spectral intensity into the nonlinear regime. An increase in the signal level reduces the susceptibility of the TLAF signal to background interference. It therefore offers the potential to improve the quality of the temperature images.

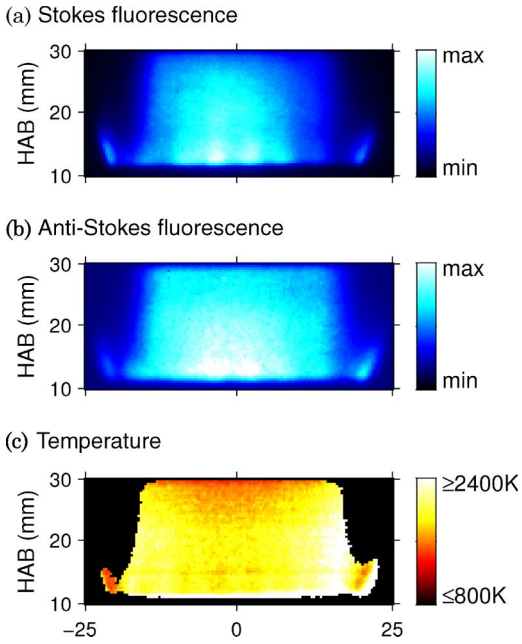

Fig. 7. (Color online) Typical averaged images of (a) Stokes and (b) anti-Stokes indium fluorescence and (c) deduced temperature in Flame 1 (Table 1). Linear fluence excitation (2500 W/cm^2/cm^{-1}). Image size approximately 20 mm × 50 mm. Laser propagation from left to right. HAB, height above burner.

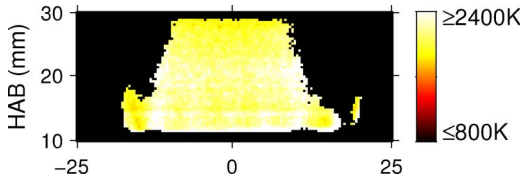

Fig. 8. (Color online) Typical deduced temperature image in Flame 2 (Table 1). Linear fluence excitation (2500 W/cm^2/cm^{-1}). Image size approximately 20 mm × 50 mm. Laser propagation from left to right. HAB, height above burner.

G. Temperature Measurement—Nonlinear Fluence

The results presented in this subsection are for nonlinear laser excitation using a 45 mm × 4.5 mm sheet with an irradiance of 2.5×10^5 W/cm^2/cm^{-1}.

1. *Natural Gas—Images*

For nonlinear excitation, Figs. 10(a) and 10(b), respectively, show typical instantaneous Stokes and anti-Stokes fluorescence images collected simultaneously for Flame 1 (Table 1). The SNR of the nonlinear images is ~25:1 for Stokes and ~15:1 for anti-Stokes, a significant improvement to that achieved in the linear regime (Subsection 4.D). Applying the derived NTLAF theory to these images yields the deduced temperature image presented in Fig. 10(c). Again, for nonlinear excitation, the SNR of the temperature image has improved to ~20:1 (~100 K), significantly higher than 8:1 (~250 K) of the linear regime.

Figure 11 presents a histogram obtained from each of the instantaneous temperature images for Flame 1 [Figs. 6(c) and 10(c)]. This also demonstrates a significant improvement in SNR, and hence a reduction in the uncertainty, by operation in the nonlinear regime. Specifically, while both the linear and the nonlinear measurements yield a mean temperature of ~1800 K, the range of measured data spans 1500–2100 K for the nonlinear measurement,

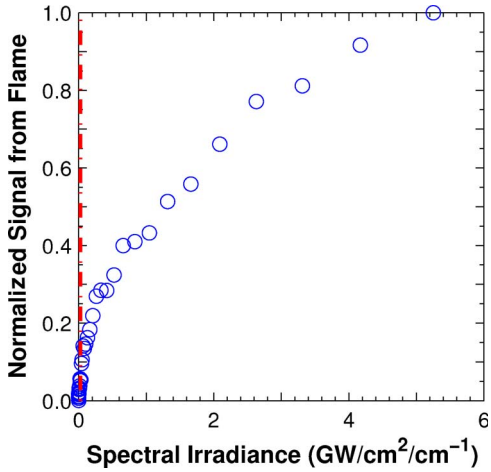

Fig. 9. (Color online) Indium fluorescence (Stokes) as a function of spectral intensity to the maximum achievable laser energy. Vertical red dashed line indicates limit of linearity (2500 W/cm^2/cm^{-1}).

approximately half of the 1200–2400 K range measured in the linear regime.

2. *Natural Gas—Stoichiometry*

The generality of the NTLAF method depends on the sensitivity of the constants in Eq. (2) to local conditions, such as species concentration. To assess the sensitivity of the NTLAF technique to the composition, the stoichiometry of a premixed natural gas/air flame was varied. This provides a range of differing concentrations of key species that may affect the NTLAF constants.

The formation of neutral indium atoms from the indium chloride is favored under fuel-rich conditions (Subsection 4.D). Figure 12 presents the Stokes and anti-Stokes fluorescence across the range of premixed natural gas/air flames achievable with the current flat-flame burner. The increase in indium atoms in fuel-rich flames can be deduced from the increase in fluorescence signal shown in Fig. 12.

Figure 13 presents the measured temperature derived over a range of stoichiometries. Included in Fig. 13 are the calibrated radiation-corrected temperature measurements using the thermocouple probe, as well as the deduced NTLAF temperature. The maximum temperature measured by NTLAF and the thermocouple is 2033 K. It is also noted that equilibrium calculations predict a maximum temperature of ~2060 K, within 30 K of the NTLAF and thermocouple measurements. A close agreement among all three techniques is noted, indicating, for the first time, the validity of the derived NTLAF derivations.

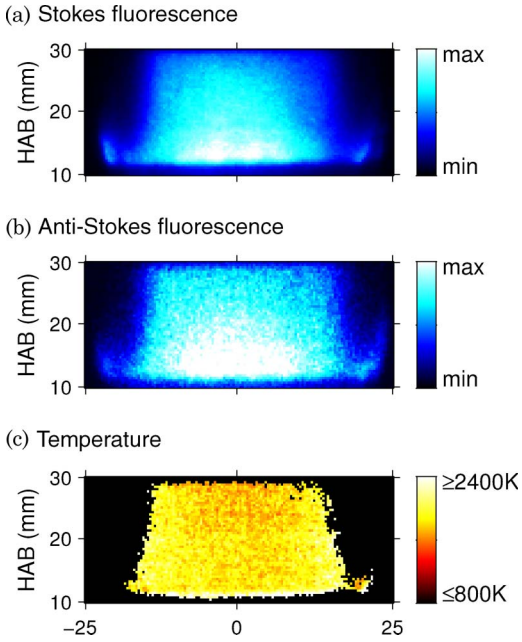

Fig. 10. (Color online) Typical instantaneous images of (a) Stokes and (b) anti-Stokes indium fluorescence and (c) deduced temperature in Flame 1 (Table 1). Nonlinear fluence excitation ($250,000\,W/cm^2/cm^{-1}$). Image size approximately 20 mm × 50 mm. Laser propagation from left to right. HAB, height above burner.

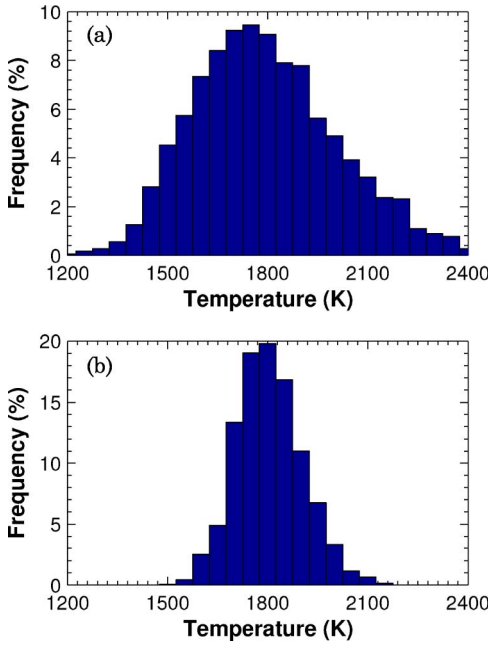

Fig. 11. (Color online) Temperature histograms from single instantaneous images of Flame 1 (Table 1) for (a) linear ($2500\,W/cm^2/cm^{-1}$) and (b) nonlinear ($250,000\,W/cm^2/cm^{-1}$) excitation regimes.

The measurements presented in Fig. 13 were obtained at a height 20 mm above the burner face. The NTLAF temperature was evaluated from the mean over a region of the images corresponding to the location of the thermocouple bead (measured separately). Also included in Fig. 13 is the standard deviation of the data obtained from 200 shots for each NTLAF data point (indicated by the error bars). The standard deviation is typically around 100 K, representing an uncertainty of approximately 5%, and is primarily due to detector noise in the image and imperfect correction of the laser beam energy and profile from the reference source (namely, the tank).

Determination of temperature by NTLAF requires calibration, which has been determined here based on the maximum temperature condition. Results at other stoichiometries have been calculated based on the single calibration point. The close agreement at the other stoichiometries ($\lesssim$20 K) suggests that the calibration constants are relatively insensitive to changes in the flame composition.

The flame stoichiometry was varied by maintaining a constant flow rate of air and nitrogen through the seeder, and adjusting the fuel flow rate. This ensures a relatively constant net flow rate and so also a consistent seeding concentration. Worth noting is that the maximum temperature is approximately 180 K below the adiabatic flame temperature for methane. This temperature drop is due to the combined effects of the nitrogen carrier gas and the effect of the water solvent used in the seeding system,

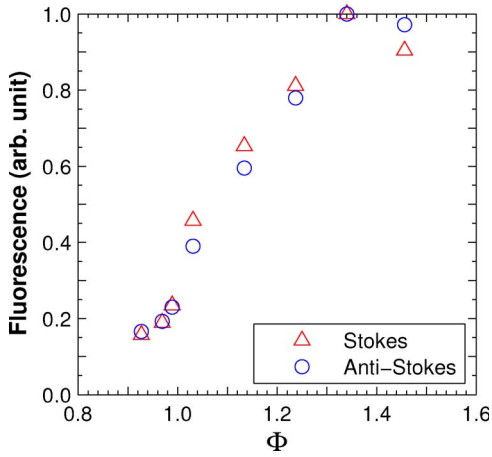

Fig. 12. (Color online) Fluorescence signal in Flame 3 (Table 1) as a function of stoichiometry (Φ).

which has been confirmed with systematic thermocouple measurements.

3. *Hydrogen—Stoichiometry*

Further assessment of the sensitivity of the calibration constants determined from the maximum temperature condition of the natural gas/air premixed flame (Subsection 4.G.2) is obtained by performing the measurements with hydrogen. Figure 14 presents the measured temperature for premixed hydrogen/air flames over a range of stoichiometries. The standard deviation (indicated by the error bars) obtained from the 200 shots at each NTLAF point is approximately 5%. Close agreement (typically less than 80 K) is again found between the thermocouple and the NTLAF measurements. Of particular note is that, although the calibration constants were determined for natural gas fuel, they also provide good results for hydrogen. This is further confirmation of the validity and wide applicability of the nonlinear theory, even with a single set of constants.

The hydrogen/air mixture can sustain flames with higher stoichiometries, and so lower temperature, than is possible for the natural gas/air case. Figure 14 demonstrates that the NTLAF technique can measure temperatures below 1000 K. Assessment of temperatures less than this cannot be achieved with the current burner.

As previously observed with the natural gas/air flames, on the lean side of stoichiometry, the indium fluorescence signal is insufficient to obtain reliable measurement of temperature using NTLAF.

As with natural gas flames, the temperatures in the seeded hydrogen/air flames are lower than those of an unseeded hydrogen/air flame. Again, this is primarily due to the introduction of nitrogen from the seeding system. For the present system, higher nitrogen dilution was required for the hydrogen flame to enable safe and reliable operation of the burner, although this is not a general requirement.

4. *Ethylene—Stoichiometry*

For a further check on the sensitivity of the calibration constants to fuel type, the measurement was also performed with ethylene. Figure 15 presents the measured temperatures for premixed ethylene/air flames over a range of stoichiometries. As before, these measurements are derived from the calibration constants obtained for natural gas (Subsection 4.G.2), and the standard deviation at each point is approximately 5%. Again, the NTLAF agrees well with the thermocouple measurements, with a difference typically not more than 40 K. The leanest ($\Phi = 0.8$) measurement shows the most variation between the NTLAF and the thermocouple, a difference of around 100 K, due to the lower signal under lean conditions.

Ethylene has a high propensity to generate soot. Flame conditions with $\Phi > 1.7$ (indicated by the vertical dashed line) visually show evidence of the presence of soot within these flames. Figure 16(a) shows a photograph of the flame with $\Phi = 2.25$. The deduced NTLAF instantaneous single-shot temperature image for this flame is presented in Fig. 16(b). The agreement between the NTLAF and the

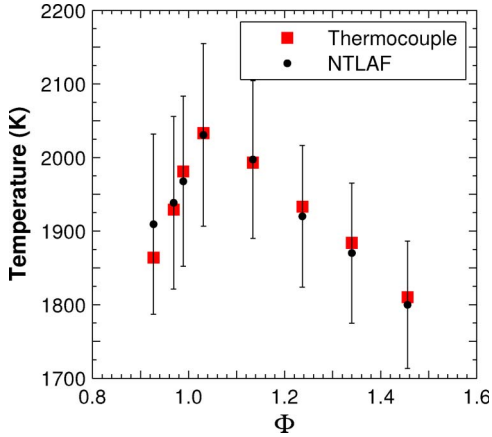

Fig. 13. (Color online) Temperature of Flame 3 (Table 1) over a range of stoichiometry (Φ) for NTLAF and calibrated thermocouple measurements.

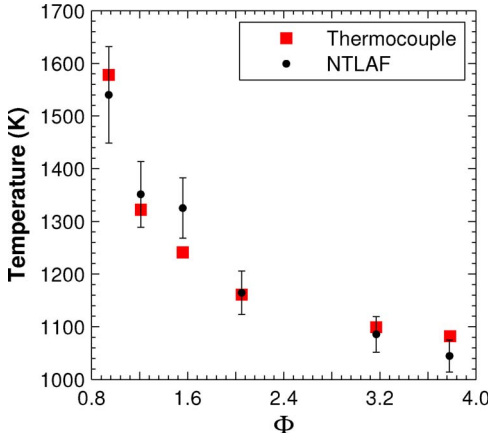

Fig. 14. (Color online) Temperature of Flame 4 (Table 1) over a range of stoichiometry (Φ) for NTLAF and calibrated thermocouple measurements.

thermocouple are independent, irrespective of the presence or absence of soot (Fig. 15). In those flames with soot, when the laser wavelength is shifted off resonance, the fluorescence signal was found to be below detectable limits, demonstrating good capacity of the present filtering to exclude soot interferences. Similarly, soot did not influence the thermocouple readings, as there was no deposition on the bead, thus not altering its emissivity.

5. Conclusion

TLAF is potentially one of the most suitable two-dimensional laser-based thermometry techniques for sooting environments. TLAF has previously been demonstrated to be feasible in sooting flames, but instantaneous imaging has been elusive. We have extended the previous TLAF derivations from linear excitation into the nonlinear fluence regime using existing theory. NTLAF provides superior signal compared to conventional linear TLAF. Comparisons of imaging using conventional TLAF to NTLAF have been presented and have shown that the SNR is improved from ~8:1 to ~20:1, leading to a reduction in the single-shot uncertainty from 250 to 100 K. Temperature imaging with an accuracy of ~100 K compares favorably to alternative thermometry techniques but with the advantage of being suited to flames containing soot.

Although NTLAF is susceptible to the effects of differing composition, the small amount of uncertainty associated with the determination of the constants is far outweighed by the ability to collect large-dimension single-shot images with superior signal, ~10 times greater for the presented work. Furthermore, this work has demonstrated the validity of the nonlinear derivations and the applicability of a single set of constants across a wide range of flame conditions. Using the calibration from a single natural gas/air premixed flame, NTLAF has been shown to resolve the temperature profile across the stoichiometric envelope for hydrogen, ethylene, and natural gas flames, with deviation from thermocouple measurements not exceeding 100 K and typically ≲30 K, which is within the experimental uncertainty.

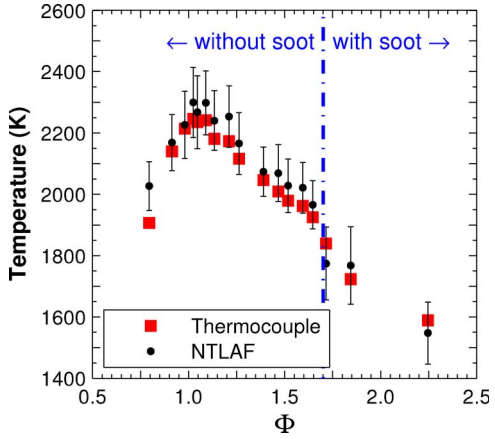

Fig. 15. (Color online) Temperature of Flame 5 (Table 1) over a range of stoichiometry (Φ) for NTLAF and calibrated thermocouple measurements.

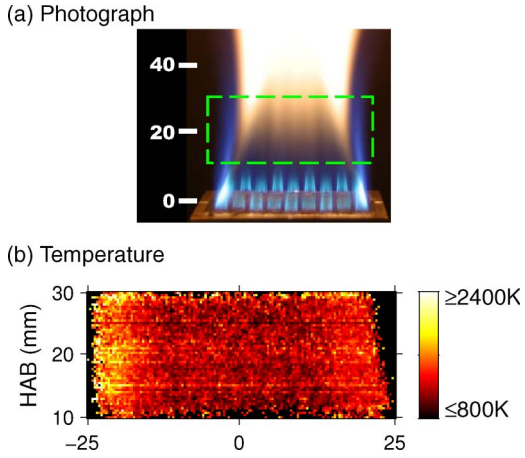

Fig. 16. (Color online) (a) Photograph of ethylene/air flame with Φ = 2.25 showing soot. Dashed area indicates approximate laser-imaging area. (b) Instantaneous NTLAF temperature image for this flame. Image size approximately 20 mm × 50 mm. Laser propagation from left to right. HAB, height above burner.

NTLAF imaging has also been applied to flames containing soot. For the soot levels of the flame conditions presented, the background interferences were below detectable limits, demonstrating good capacity of filtering to exclude soot interferences. This also further indicates the ability to use a single set of NTLAF constants for different flame conditions, including in the presence of soot.

Appendix A: Nonlinear Two-Line Atomic Fluorescence Derivation

Referring to Fig. 1, the rate equation for pumping to level 2 via optical absorption from lower state i (namely, $i = 0$ or 1) is given by [9]

$$\frac{dN_2}{dt} = N_i(Q_{i2} + B_{i2}I_{i2}) - N_2(B_{2i}I_{2i} + Q_{20} + Q_{21} + A_{20} + A_{21}). \quad \text{(A1)}$$

The subscripts refer to the transition between the energy levels, N is the population in energy level, Q is the nonradiative rate constant, A is the transition probability coefficient for spontaneous absorption or emission, B is the transition probability coefficient for stimulated absorption or emission, and I is the incident laser spectral irradiance. Following excitation, the fluorescence process from level 2 to lower state i may be described [9] by

$$F_{2i} = h\nu_{2i}N_2A_{2i}\frac{\Omega}{4\pi}V, \quad \text{(A2)}$$

where F is the fluorescence, $h\nu$ is the photon energy, Ω is the collection solid angle, and V is the probe volume. Taking the ratio of the two fluorescence signals gives

$$\frac{F_{20}}{F_{21}} = \frac{h\nu_{20}\frac{\Omega_{20}\varepsilon_{20}}{4\pi}\frac{N_1 B_{12} I_{12} A_{20}}{B_{21} I_{21} + Q + A}}{h\nu_{21}\frac{\Omega_{21}\varepsilon_{21}}{4\pi}\frac{N_0 B_{02} I_{02} A_{21}}{B_{20} I_{20} + Q + A}}, \tag{A3}$$

where ε represents the collection efficiency. The numerator of Eq. (A3) may be reexpressed as

$$F_{20} = h\nu_{20}\frac{\Omega_{20}\varepsilon_{20}}{4\pi} N_1 A_{20}\frac{B_{12}}{B_{21}}\frac{1}{1+\frac{Q+A}{B_{21}I_{21}}}, \tag{A4}$$

and noting that

$$g_i B_{ij} = g_j B_{ji}, \tag{A5}$$

gives

$$F_{20} = h\nu_{20} A_{20} N_1 \frac{\Omega_{20}\varepsilon_{20}}{4\pi}\frac{g_2}{g_1}\frac{1}{1+\frac{Q+A}{B_{21}I_{21}}}. \tag{A6}$$

Applying the same rearrangement to the denominator, Eq. (A3) can now be expressed as the ratio

$$\frac{F_{20}}{F_{21}} = \frac{\nu_{20}\Omega_{20}\varepsilon_{20}A_{20}N_1 g_0}{\nu_{21}\Omega_{21}\varepsilon_{21}A_{21}N_0 g_1}\left(\frac{1+\frac{Q+A}{B_{20}I_{20}}}{1+\frac{Q+A}{B_{21}I_{21}}}\right). \tag{A7}$$

Using the previously defined C_S and C_A [Eqs. (3) and (4)] allows Eq. (A7) to be written as

$$\frac{F_{20}}{F_{21}} = \frac{\nu_{20}\Omega_{20}\varepsilon_{20}A_{20}N_1 g_0}{\nu_{21}\Omega_{21}\varepsilon_{21}A_{21}N_0 g_1}\left(\frac{1+\frac{C_S}{I_{20}}}{1+\frac{C_A}{I_{21}}}\right). \tag{A8}$$

Applying the Boltzmann function yields

$$\frac{F_{20}}{F_{21}} = \frac{\nu_{20}\Omega_{20}\varepsilon_{20}A_{20}}{\nu_{21}\Omega_{21}\varepsilon_{21}A_{21}}\left(\frac{1+\frac{C_S}{I_{20}}}{1+\frac{C_A}{I_{21}}}\right)e^{-\Delta E_{10}/kT}. \tag{A9}$$

Taking the natural logarithm and rearranging leaves

$$\frac{\Delta E_{10}}{kT} = \ln\left(\frac{F_{21}}{F_{20}}\right) + C_T + \ln\left(1+\frac{C_S}{I_{20}}\right) - \ln\left(1+\frac{C_A}{I_{21}}\right). \tag{A10}$$

Expressing the temperature explicitly leaves Eq. (2) as

$$T = \frac{\Delta E_{10}/k}{\ln\left(F_{21}\times\left(1+\frac{C_S}{I_{20}}\right)\right) - \ln\left(F_{20}\times\left(1+\frac{C_A}{I_{21}}\right)\right) + C_T}. \tag{A11}$$

The authors thank the Fluid-MEC group at the University of Adelaide and the Australian Research Council for funding support through ARC Discovery and LIEF grant schemes.

References

1. M. A. Delichatsios, J. De Ris, and L. Orloff, "An enhanced flame radiation burner," Proc. Combust. Inst. **24**, 1075–1082 (1992).
2. C. R. Shaddix and T. C. Williams, "Soot: giver and taker of light," Am. Sci. **95**, 232–239 (2007).
3. Z. A. Mansurov, "Soot formation in combustion processes," Combust. Explos. Shock Waves (English translation) **41**, 727–744 (2005).
4. D. W. Dockery and P. H. Stone, "Cardiovascular risks from fine particulate air pollution," N. Engl. J. Med. **356**, 511–513 (2007).
5. K. A. Miller, D. S. Siscovick, L. Sheppard, K. Shepherd, J. H. Sullivan, G. L. Anderson, and J. D. Kaufman, "Long-term exposure to air pollution and incidence of cardiovascular events in women," N. Engl. J. Med. **356**, 447–458 (2007).
6. R. M. Frinstrom and A. A. Westenberg, *Flame Structure* (McGraw-Hill, 1965).
7. K. Kohse-Höinghaus and J. B. Jeffries, *Applied Combustion Diagnostics* (Taylor & Francis, 2002).
8. A. T. Hartlieb, B. Atakan, and K. Kohse-Höinghaus, "Temperature measurement in fuel-rich non-sooting low pressure hydrocarbon flames," Appl. Phys. B **70**, 435–445 (2000).
9. A. C. Eckbreth, *Laser Diagnostics for Combustion Temperature and Species* (Gordon & Breach, 1996).
10. D. Hoffman, K.-U. Münch, and A. Leipertz, "Two-dimensional temperature determination in sooting flames by filtered Rayleigh scattering," Opt. Lett. **21**, 525–527 (1996).
11. D. Hofmann and A. Leipertz, "Temperature field measurements in a sooting flame by filtered Rayleigh scattering (FRS)," Proc. Combust. Inst. **26**, 945–950 (1996).
12. S. P. Kearney, R. W. Schefer, S. J. Beresh, and T. W. Grasser, "Temperature imaging in nonpremixed flames by joint filtered Rayleigh and Raman scattering," Appl. Opt. **44**, 1548–1558 (2005).
13. M. Afzelius, P.-E. Bengtsson, J. Bood, C. Brackmann, and A. Kurtz, "Development of multipoint vibrational coherent anti-Stokes Raman spectroscopy for flame applications," Appl. Opt. **45**, 1177–1186 (2006).
14. R. Cattolica, "OH rotational temperature from two-line laser-excited fluorescence," Appl. Opt. **20**, 1156–1166 (1981).
15. W. Qin, Y.-L. Chen, and J. W. L. Lewis, "Time-resolved temperature images of laser-ignition using OH two-line laser-induced fluorescence (LIF) thermometry," Tech. Rep. Article Number 200508, IFRF Combustion Journal (2005).
16. J. M. Seitzman, R. K. Hanson, P. A. DeBarber, and C. F. Hess, "Application of quantitative two-line OH planar laser-induced fluorescence for temporally resolved planar thermometry in reacting flows," Appl. Opt. **33**, 4000–4012 (1994).
17. J. Nygren, J. Engström, J. Walewski, C. F. Kaminski, and M. Aldén, "Applications and evaluation of two-line atomic LIF thermometry in sooting combustion environments," Meas. Sci. Technol. **12**, 1294–1303 (2001).
18. M. Haudiquert, A. Cessou, D. Stepowski, and A. Coppalle, "OH and soot concentration measurements in a high-temperature laminar diffusion flame," Combust. Flame **111**, 338–349 (1997).
19. M. Tamura, J. Luque, J. E. Harrington, P. A. Berg, G. P. Smith, J. B. Jeffries, and D. R. Crosley, "Laser-induced fluorescence of seeded nitric oxide as a flame thermometer," Appl. Phys. B **66**, 503–510 (1998).
20. W. G. Bessler, F. Hildenbrand, and C. Schulz, "Two-line laser-induced fluorescence imaging of vibrational temperatures in a NO-seeded flame," Appl. Opt. **40**, 748–756 (2001).
21. H. Kronemayer, P. Ifeacho, C. Hecht, T. Dreier, H. Wiggers, and C. Schulz, "Gas-temperature imaging in a low-pressure flame reactor for nano-particle synthesis with multi-line NO-LIF thermometry," Appl. Phys. B **88**, 373–377 (2007).

22. T. Lee, J. B. Jeffries, and R. K. Hanson, "Experimental evaluation of strategies for quantitative laser-induced fluorescence imaging of nitric oxide in high-pressure flames (1–60 bar)," Proc. Combust. Inst. **31**, 757–764 (2007).
23. B. Atakan and A. T. Hartlieb, "Laser diagnostics of NO reburning in fuel-rich propene flames," Appl. Phys. B **71**, 697–702 (2000).
24. M. Aldén, P. Grafström, H. Lundberg, and S. Svanberg, "Spatially resolved temperature measurements in a flame using laser-excited two-line atomic fluorescence and diode-array detection," Opt. Lett. **8**, 241–243 (1983).
25. R. G. Joklik and J. W. Daily, "Two-line atomic fluorescence temperature measurement in flames: an experimental study," Appl. Opt. **21**, 4158–4162 (1982).
26. H. Haraguchi and J. D. Winefordner, "Flame diagnostics: local temperature profiles and atomic fluorescence intensity profiles in air-acetylene flames," Appl. Spectrosc. **31**, 195–200 (1977).
27. J. Engström, J. Nygren, M. Aldén, and C. F. Kaminski, "Two-line atomic fluorescence as a temperature probe for highly sooting flames," Opt. Lett. **25**, 1469–1471 (2000).
28. H. Haraguchi, B. Smith, S. Weeks, D. J. Johnson, and J. D. Winefordner, "Measurement of small volume flame temperatures by the two-line atomic fluorescence method," Appl. Spectrosc. **31**, 156–163 (1977).
29. C. F. Kaminski, J. Engström, and M. Aldén, "Quasi-instantaneous two-dimensional temperature measurements in a spark ignition engine using 2-line atomic fluorescence," Proc. Combust. Inst. **27**, 85–93 (1998).
30. C. T. J. Alkemade, "A theoretical discussion on some aspects of atomic fluorescence spectroscopy in flames," Pure Appl. Chem. **23**, 73–98 (1970).
31. J. E. Dec and J. O. Keller, "High speed thermometry using two-line atomic fluorescence," Proc. Combust. Inst. **21**, 1737–1745 (1986).
32. J. Hult, I. S. Burns, and C. F. Kaminski, "Two-line atomic fluorescence flame thermometry using diode lasers," Proc. Combust. Inst. **30**, 1535–1543 (2005).
33. I. S. Burns, J. Hult, and C. F. Kaminski, "Spectroscopic use of a novel blue diode laser in a wavelength region around 450 nm," Appl. Phys. B **79**, 491–495 (2004).
34. I. S. Burns, J. Hult, G. Hartung, and C. F. Kaminski, "A thermometry technique based on atomic lineshapes using diode laser LIF in flames," Proc. Combust. Inst. **31**, 775–782 (2007).
35. J. E. Sansonetti and W. C. Martin, "Handbook of basic atomic spectroscopic data," J. Phys. Chem. Ref. Data **34**, 1559–2259 (2005).
36. R. K. Winge, V. A. Fassel, and R. N. Kniseley, "Direct nebulization of metal samples for flame atomic-emission and absorption spectroscopy," Appl. Spectrosc. **25**, 636–642 (1971).
37. P. A. Bonczyk, "Effects of metal additives on soot precursors and particulates in a $C_2H_4/O_2/N_2/Ar$ premixed flame," Fuel **70**, 1403–1411 (1991).
38. U. Wieschnowsky, H. Bockhorn, and F. Fetting, "Some new observations concerning the mass growth of soot in premixed hydrocarbons-oxygen flames," Proc. Combust. Inst. **22**, 343–352 (1988).
39. B. S. Haynes, H. Jander, and H. G. Wagner, "The effect of metal additives on the formation of soot in premixed flames," Proc. Combust. Inst. **17**, 1365–1374 (1979).
40. J. A. Dean and T. C. Rains, *Flame Emission and Atomic Absorption Spectrometry* (Marcel Dekker, 1969), Vol. 1.